Considerations on seismic microzonation in areas with two-dimensional hills

Mohsen Kamalian[1], Abdollah Sohrabi-Bidar[2], Arash Razmkhah[3], Amirata Taghavi[4] and Iraj Rahmani[5]

[1] *Geotechnical Engineering Research Center, International Institute of Earthquake Engineering and Seismology, 26 Arghavan St., North Dibajee, Farmanieh, Tehran, I.R. Iran.*
[2] *Seismology Research Center, International Institute of Earthquake Engineering and Seismology, 26 Arghavan St., North Dibajee, Farmanieh, Tehran, I.R. Iran.*
[3] *Civil Engineering Department, Faculty of Engineering, Islamic Azad University, South of Tehran Campus, Ahang Highway, Abouzar Building, Afsarieh Highway, Tehran, I.R. Iran.*
[4] *Civil Engineering Department, Iran University of Science and Technology, Narmak, Tehran, I.R. Iran.*
[5] *Transportation Research Institute, No. 19, Noor Street, Afrigha Avenue, Tehran, I.R. Iran.*

This paper presents the results of an extensive numerical parametric study on seismic behavior of 2D homogenous hills subjected to vertically propagating incident SV waves. It is shown that the amplification potential of these hills is strongly influenced by the wavelength, by the shape ratio, by the shape of the hill and in a less order of importance, by the Poisson ratio of the media. The 2D topography effect could be ignored, only if the hill has a shape ratio of less than 0.1 or if it is subjected to incident waves with predominant dimensionless periods of greater than 13 times the shape ratio. In incidence of waves with wavelengths longer than the width of the hill, the amplification curve usually finds its maximum at the crest and decreases towards the base of the hill. Else, some de-amplification zones would occur along the hill. Among hills with similar shape ratios, those with intermediate cross section areas show intermediate seismic behavior, too. Estimated seismic site coefficients for the crest of a 2D rocky hill depend on its shape ratio and could reach even 1.7, which encourages one to classify it according to standard site categorization procedures as soil profile types SC or SD instead of the conventional SB type.

1. Introduction

In the current practice of 1D numerical seismic microzonation, it is usually assumed that the incident body shear waves propagate in the vertical direction and that any rock-like outcrop irrespective of the ground surface irregularities constitutes part of the amplification-free reference site (TC4 1993). Figure 1 presents a schematic view of some typical sites encountered frequently in seismic microzonation studies. Points A, B, C and D indicate, respectively, the ground surface of a soil stratum consisting of multiple layers with different mechanical properties overlying the bedrock, the rock outcrop on the flat half-plane, which is conventionally considered as the reference site and two arbitrary points along the homogenous rocky hill. However, the following questions arise in this regard: Is it always reasonable and conservative to consider points C and D (toe and crest of the rocky hill) as parts of the amplification-free reference site? When is it necessary in seismic microzonation studies to consider the topography effect? Does any simple formula exist to enable one to modify the 1D seismic microzonation results for the 2D topography effects?

In the recent past, there have been numerous cases of recorded motion and observed earthquake

Keywords. Site effect; topography effect; two-dimensional hill; characteristic period; amplification; microzonation; design spectra; shape ratio; shape of the hill.

J. Earth Syst. Sci. **117**, S2, November 2008, pp. 783–796

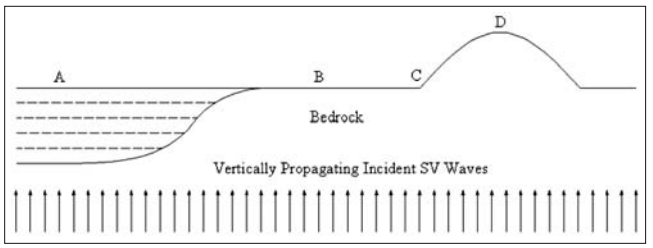

Figure 1. A schematic view of different site effect conditions subjected to the same incident waves. Points A, B, C and D respectively indicate, the ground surface of a soil stratum consisting of multiple layers with different mechanical properties overlying the bedrock, the outcrop of the rock on the flat half-plane, toe of the homogenous rocky hill and the crest of the hill.

damage pointing toward topographic amplification as an important effect. Very high accelerations recorded at the Pacoima Dam (1.25 g) during the 1971 San Fernando earthquake (Trifunac and Hudson 1971; Boore 1973) and at the Tarzana hill (1.78 g) during the 1994 Northridge earthquake (Spudich *et al* 1996) have been at least partly attributed to topographic effects. Observations from the 1983 Coalinga earthquake (Celebi 1991), the 1985 Chile earthquake (Celebi 1987), the 1987 Superstition Hills earthquake (Celebi 1991) as well as observations from recent earthquakes in Greece (Athanasopoulos *et al* 1999; Bouckovalas and Kouretzis 2001) are only some examples of catastrophic events, during which severe structural damage has been reported on high elevated regions.

Although nowadays it is well established that the seismic ground response of surface topographies could be different compared to those of the free field motion during earthquakes, there are only few structural codes, which have considered this issue (AFPS 1990; Eurocode 8 1998). This is because conclusive results from only field measurements are difficult to obtain. Indeed, because of the complexity of wave scattering phenomena, produced by the topographic structures, the problem can only be solved accurately, economically and under realistic conditions by advanced numerical methods. Beskos (1987, 1997), Sánchez-Sesma (1987) and Sánchez-Sesma *et al* (2002), have presented a compilation of works on the numerical modeling of seismic wave propagation.

In site response analyzing of the two-dimensional hills, Boore (1972) was the first who investigated the seismic response of triangular shaped hills subjected to incident SH wave. Using finite deference method, Boore showed that, effects of topography could be quite important in determining the spatial distribution of acceleration. Bouchon (1973) investigated the seismic response of semi-sine shaped hills subjected to incident SH, SV and P waves, using the well-known frequency domain Aki and Larner method (1970). Although he carried out an interesting parametric study on the hills with different shape ratios (height to half width ratio of the hill), his published results were restricted to the special case of the incident SH wave. Bard (1982) applied the Aki–Larner method to solve the scattering and diffraction of P and SV waves by surface topographies. Sánchez-Sesma (1983) applied a boundary method based on wave expansion to solve the scattering and diffraction of SH wave by triangular shaped hills. Bouchon (1985) and Gaffet and Bouchon (1989) applied discrete wave-number boundary element method to solve the scattering of SH, SV and P waves by surface irregularities. Later Geli *et al* (1988), using the Aki–Larner method, studied the combined effects of subsurface layering and neighboring ridges on seismic behavior of 2D semi-sine shaped hills. However, their study was restricted to a single shape ratio and special case of the incident SH wave. Sánchez-Sesma and Campillo (1991, 1993) were the first who investigated the seismic response of 2D semi-elliptical and triangular shaped hills, using boundary element method in frequency domain. Although they considered both cases of the incident SV and P waves, their study was restricted to only one shape ratio and one Poisson ratio. Pederson *et al* (1994) extended boundary element method in frequency domain for three-dimensional scattering of two-dimensional topographies and studied seismic behavior of a semi-circular shaped hill to different incident and azimuth angles. Takenaka *et al* (1996) extended discrete wave-number boundary element method to solve the three-dimensional scattering by two-dimensional surface irregularities. They solved the scattering and diffraction of point source generated waves by a two-dimensional semi-sine shaped hill. Zhang *et al* (1998) used a hybrid discrete wave-number boundary element/finite element method to solve the three-dimensional scattering by two-dimensional surface irregularities. They solved the scattering and diffraction of SH wave by a two-dimensional hill. Moczo *et al* (1997), using a hybrid finite deference/discrete wavenumber method, studied the scattering and diffraction of SV wave by a two-dimensional trapezoidal hill. Later Kamalian *et al* (2003a, b, 2006) applied the time domain boundary element method and the hybrid time domain boundary element/finite element method to analyse the scattering and diffraction of P and SV waves by homogenous and non-homogenous topographic structures. They executed site response analysis of 2D semi-sine, trapezoidal and semi-circular shaped hills subjected to vertically propagating SV and P incident waves.

Review of the literature shows that perfect parametric studies on seismic behavior of 2D hills subjected to incident SV waves have been seldom published. The published works were either limited to the simple and less critical case of incident SH waves or were restricted to some specific shapes and some specific values of shape ratio and predominant frequency. Furthermore, a few other published works presented interesting parametric analysis on the site response of topographic structures (Zhang and Zhao 1988; Zhao and Valliappan 1993; Ashford *et al* 1997; Bouckovalas and Papadimitriou 2005; Kamalian *et al* 2007), were only focused on the seismic behavior of slopes and valleys.

This paper presents the results of a numerical parametric study on amplification pattern of 2D homogenous hills subjected to vertically propagating incident SV waves. The study is performed using the time-domain boundary element (BE) method. Owing to the fact that incident P and SH waves have less important effect on 2D hills compared to the SV wave (Geli *et al* 1988), they are not included in this paper. The main essence of this paper is to present a clear perspective of amplification patterns of 2D hills and assessing the effects of wave characteristics, site geometry and geomechanical parameters on the amplification potential of 2D hills. In addition, some simple preliminary formula and tables are obtained which could be used as starting points in estimation of the amplification potential of the hills as well as site coefficients in seismic microzonation studies of topographic areas.

2. Methodology of parametric analysis

The parametric study was aimed at finding out answers to the following questions: What is the maximum amplification potential of the hill and where does it occur? How does the amplification pattern vary along the hill? If the same hill is subjected to incident waves with different wavelengths, how does its amplification potential change? If some hills with different shape ratios but similar shapes are subjected to the same incident wave, how do their amplification potentials differ? Could some limiting height or wavelength be introduced behind which the topography effect could be ignored? If some hills with different shapes but similar shape ratios are subjected to the same incident wave, how do their amplification potentials differ?

In order to find out answers to the above-mentioned questions, the seismic behavior of trapezoidal, semi-sine and semi-elliptical shaped 2D hills were investigated. In the case of trapezoidal hills four distinct shape ratios of 0.1, 0.3, 0.5 and 0.7, in the case of semi-sine shaped hills, seven different shape ratios of 0.1 to 0.7 and in the case of semi-elliptical shaped hills four distinct shape ratios of 0.1, 0.4, 0.7 and 1.0, were analysed. The material behavior of the media was assumed linear elastic and four different Poisson ratios of 0.1, 0.2, 0.33 and 0.4 were considered. Formulas used for definition of geometry and cross section area of the hills are presented in table 1. Figure 2 compares the cross section of the above-mentioned hills *versus* different shape ratios.

The numerical parametric study was performed using the following well-known transient boundary integral equation governing the dynamic equilibrium of isotropic elastic media (Kamalian *et al* 2006, 2007):

$$c_{ij}(\xi)\cdot u_i(\xi,t) = \int_\Gamma (G_{ij} * t_i(x,t) - F_{ij} * u_i(x,t))\cdot d\Gamma, \quad (1)$$

where u_i denotes the displacement vector and t_i represents the traction at the boundary. G_{ij} and F_{ij} are the transient displacement and traction kernels respectively, and represent the displacements and tractions at a point x at time t due to a unit

Table 1. *Geometries and cross section areas of trapezoidal, semi-sine and semi-elliptical shaped hills.*

Shape	Geometry*		Cross section area
Semi-sine	$\lvert x\rvert \le b$:	$\xi(x) = 0.5h(1+\cos(\pi x/b))$	$S = SR\cdot b^2$
	$\lvert x\rvert \ge b$:	$\xi(x) = 0$	
Semi-elliptical	$\lvert x\rvert \le b$:	$\xi(x) = h\sqrt{1-(x^2/b^2)}$	$S = \frac{\pi}{2}SR\cdot b^2$
	$\lvert x\rvert \ge b$:	$\xi(x) = 0$	
Trapezoidal hill	Flank angle of 45°		$S = (2-SR)\cdot SR\cdot b^2$

*Parameters b and h denote the half-width and height of the hills, respectively, and $SR = h/b$ denotes the shape ratio.

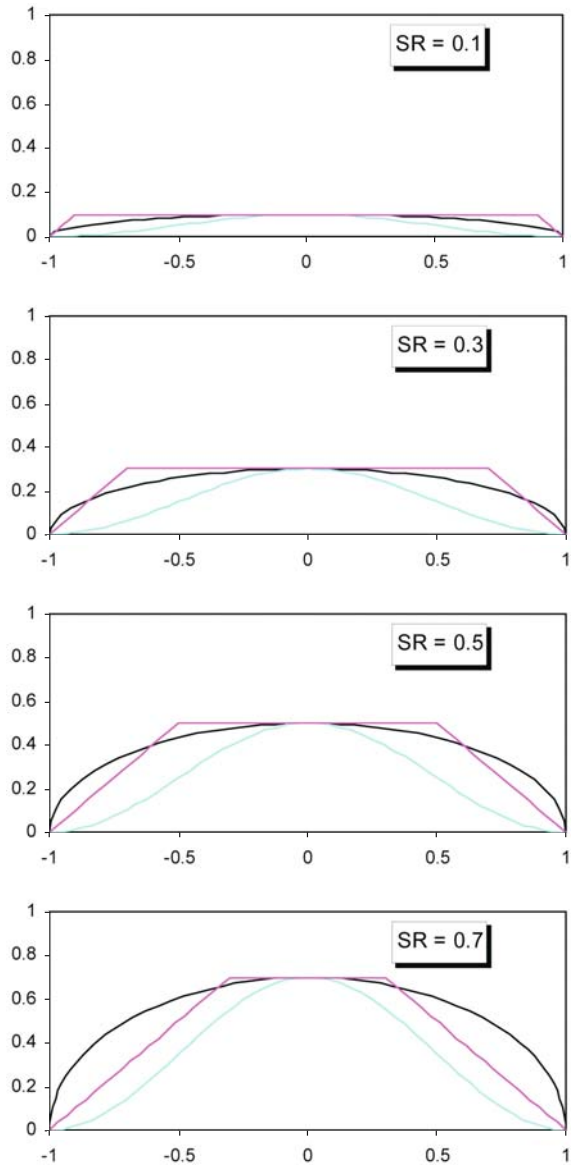

Figure 2. Comparison between cross sections of the semi-sine, trapezoidal and semi-elliptical hills. In the two first shape ratios, the trapezoidal and in the two last shape ratios, the semi-elliptical cross section has the largest area. In all of the cases, the semi-sine cross section has the smallest area.

point force applied at ξ and at the preceding time τ. The terms $G_{ij} * t_i$ and $F_{ij} * u_i$ are the Riemann convolution integrals and c_{ij} denotes the well-known discontinuity term resulting from the singularity of the F_{ij} kernel. The BE formulation of equation (1) was implemented in a general purpose two-dimensional nonlinear two-phase BEM/FEM code named as HYBRID (Kamalian 2001 and Kamalian *et al* 2003a, b, 2006, 2007).

Results in time-domain have been shown in dimensionless forms. In time-domain the dimensionless time is defined as $T = tc_2/2b$, where t, b and c_2 denote time, half width and shear wave velocity of the hill, respectively. In addition, all results in frequency-domain have been presented in dimensionless forms, using the dimensionless frequency or its inverse, the dimensionless period. The dimensionless frequency is defined as the ratio of the width of the hill to the wavelength of the shear wave, $\Omega = \omega b/\pi c_2$, where ω presents the angular frequency of the wave.

The hills were subjected to vertically propagating incident SV wave of the Ricker type:

$$f(t) = [1-2\cdot(\pi\cdot f_p\cdot(t-t_0))^2]\exp^{-(\pi\cdot f_p\cdot(t-t_0))^2}, \quad (2)$$

in which f_p and t_0 denote the predominant frequency and an appropriate time shift parameter, respectively. In all cases, the incident Ricker wave had a predominant dimensionless frequency of 1.5 and a dimensionless time shift parameter of 0.9.

Based on engineering interests, a dimensionless period interval of 0.25 to 8.33 was considered, which corresponds to incident waves with wavelengths of 0.25 to 8.33 times the width of the hill. This broad period interval was divided into the following five subintervals: 0.25 to 0.50 (P1), 0.50 to 1.00 (P2), 1.00 to 2.00 (P3), 2.00 to 4.17 (P4) and 4.17 to 8.33 (P5), corresponding to incident waves with very short, short, medium, large and very large wavelengths, respectively. The amplification curves were attained by dividing the Fourier amplitude of the horizontal component of the motion to the relevant Fourier amplitude in the free field motion. By averaging the corresponding amplification curve over the short, intermediate, mid and long period bands (P1 to P5), five distinct spectral ratios were obtained for every point along the hill. The calculated amplification factors are called 'AHSA', average horizontal spectral amplification (Borcherdt *et al* 1991, Borcherdt 1994).

3. General amplification pattern

Figures 3 and 4 show the time domain response and the amplification pattern of a 2D semi-elliptical shaped hill subjected to a vertically propagating incident SV wave, respectively. The hill has a shape ratio of 0.7 and a Poisson ratio of 0.33. The receiving points are arranged within an interval of $-4b$ to $4b$ from the crest of the hill.

Considering amplification pattern of the hill, at any point on the ground surface, irrespective of being on the hill or on the half-plane, the total motion differs from the free field motion (twice the incident motion). The motion may be amplified or de-amplified, depending on the predominant frequency of the incident wave. Moreover, both horizontal and vertical components of

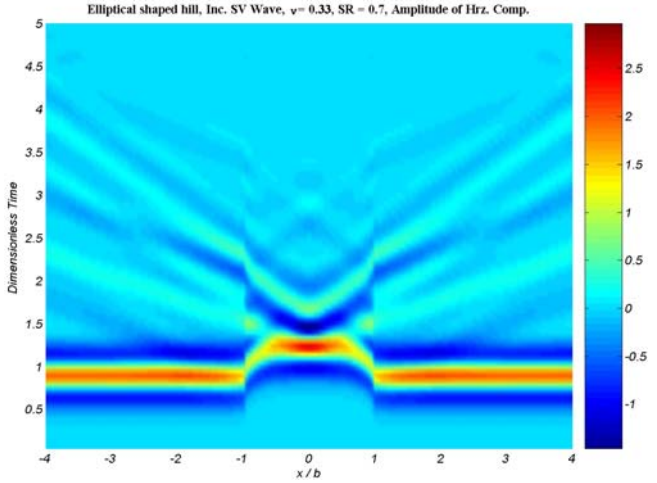

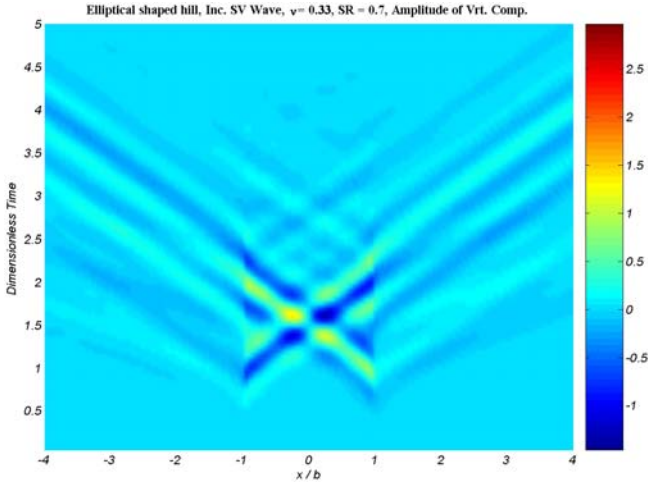

Figure 3. Incidence of a vertically propagating plane SV wave. Synthetic seismogram for surface receivers between $x = -4b$ and $x = 4b$ at surface of a 2D semi-elliptical shaped hill with a shape ratio of 0.7 and a Poisson ratio of 0.33. (top) and (bottom) horizontal and vertical components of motion, respectively. The incidence time signal is a Ricker wavelet with predominant dimensionless frequency of 1.5 and a dimensionless time shift parameter of 0.9. Different colours indicate the time domain normalized displacements (ratio of the displacement on the hill to the maximum amplitude of input Ricker wave) along the hill.

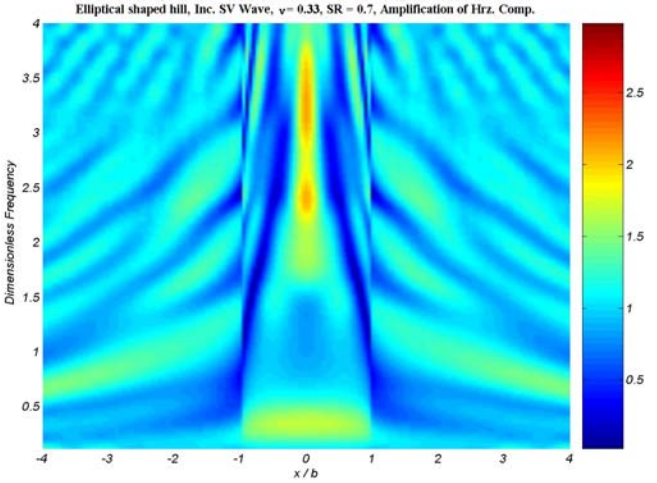

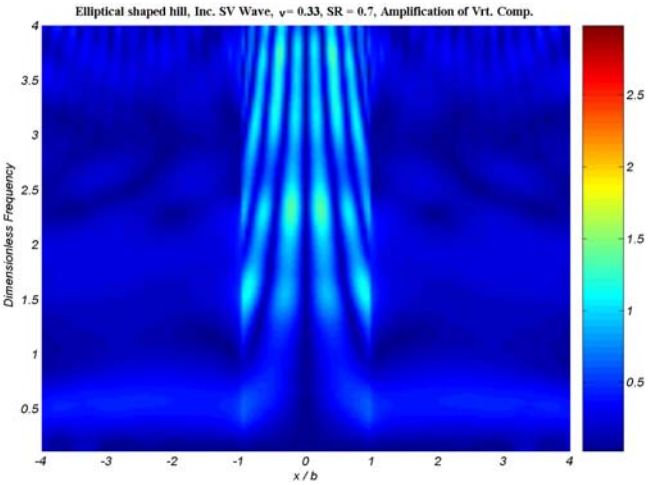

Figure 4. Incidence of a vertically propagating plane SV wave. Amplification pattern for surface receivers between $x = -4b$ and $x = 4b$ at surface of a 2D semi-elliptical shaped hill with a shape ratio of 0.7 and a Poisson ratio of 0.33. (top) and (bottom) horizontal and vertical components of motion, respectively. The incidence time signal is a Ricker wavelet with predominant dimensionless frequency of 1.5 and a dimensionless time shift parameter of 0.9. Different colours indicate the amplification values in frequency domain.

motion exist and the amplification curve consists of sequential amplifications and de-amplifications. The amplification pattern of the hill shows the existence of a characteristic frequency (or period). In characteristic frequency (or period), all points along the hill show in phase motions with amplification factors of greater than one; the amplification potential of the hill reaches its maximum; and at the last but not the least, the amplification curve of the hill finds its maximum at the crest and decays towards the bases. If the incident wave has a predominant frequency of smaller than the characteristic frequency of the hill, decreasing the frequency of the wave reduces the effect of the hill on the ground response. In other words, if the hill was impinged by incident waves with wavelengths much greater than the width of the hill, the ground surface response would be approximately the same as the well-known free field motion. It is worth noting that such conditions could occur in far-field earthquakes and in rigid like media.

4. Results of parametric analysis

This section presents results of a comprehensive parametric study on effects of wavelength of the incident wave, shape ratio of the hill, shape of the hill and Poisson ratio of media on amplification patterns of 2D hills.

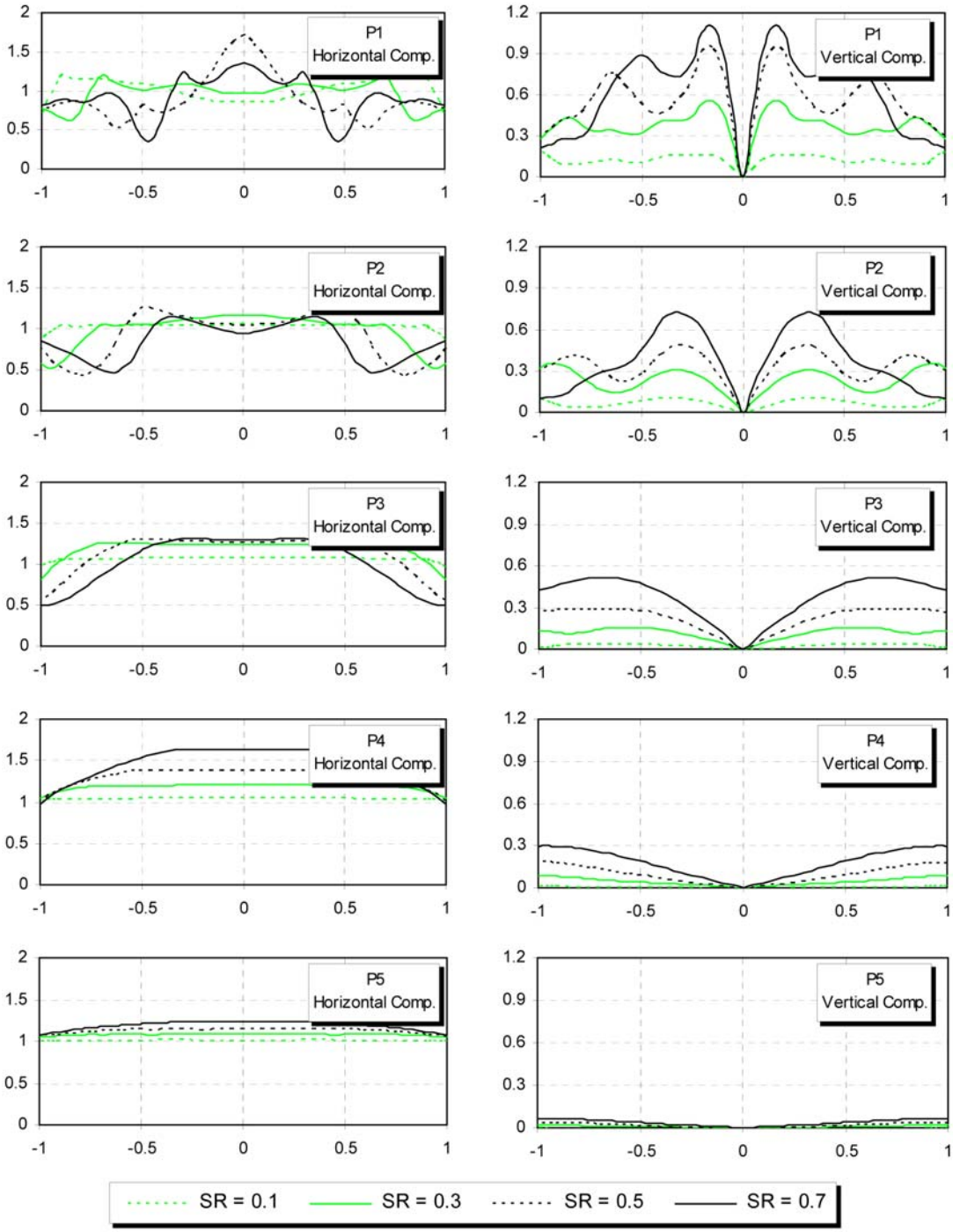

Figure 5. Incidence of a vertically propagating plane SV wave. The horizontal and vertical components of amplification curves for receivers between $x = -b$ and $x = b$ at surface of 2D trapezoidal shaped hills with different shape ratios and a Poisson ratio of 0.33. The amplification curves are categorized according to the wavelength of the incident wave.

4.1 *Wavelength effect*

Figure 5 demonstrates the dependency of the amplification potential of a 2D trapezoidal hill on the wavelength and shape ratio. The hill has a Poisson ratio of 0.33 and is subjected to vertically propagating incident SV waves. The amplification curves are categorized according to the wavelength of the incident waves. Both horizontal and vertical components of amplification are shown. As can be seen, irrespective of the shape ratio, the wavelength plays a key rule in determining the amplification curve of the hill.

Regarding the horizontal component of the motion, if the incident wave possesses a long or very long wavelength, each point across the hill

will experience amplification factor of greater than one increasing with shape ratio. Furthermore, the maximum amplification factor occurs at the top of the hill and the amplification curve decays towards the bases. In the case of an incident wave with a medium wavelength, although the same behavior would be seen, some de-amplification would also occur at the bases, whose magnitude increases with the shape ratio. In an incident wave with a short or very short wavelength, the number of de-amplification zones along the hill would increase. In this case, each point across the hill experiences its maximum amplification factor in medium shape ratios. In addition, the amplification curves of the hill may experience their maximum at points other than the crest.

Concerning the vertical component, irrespective of the shape ratio, amplification curves start from a value of zero at the top, increase with distance from the crest; reach their maximum at a point on the flank and decay towards the base. In general, at any point across the hill, the vertical amplification factor increases with the shape ratio and decreases by increasing the wavelength.

4.2 *Shape ratio effect*

Figure 5 compares the amplification curves of 2D trapezoidal shaped hills with different shape ratios. The hills are subjected to the same vertically propagating incident SV waves. As can be seen, the shape ratio as well as the wavelength of the incident wave determines the amplification potential of the hill. In general, the amplification or de-amplification potential of the hill increases with the shape ratio; however the increasing rate depends on the wavelength and varies along the hill. In other words, increasing the shape ratio (height) of the hill does not necessarily mean intensifying the amplification potential of all points along it by the same amount. In the case of hills with a shape ratio of less than 0.1, the topography effect could be ignored. Although it seems very difficult to express the amplification factor of an arbitrary point on the hill as a mathematical function of its location, shape ratio and wavelength of incident wave, but some meaningful engineering indexes could be evaluated only as a function of the shape ratio.

Figure 6 depicts the amplification curves of the crest of 2D trapezoidal hills *versus* the shape ratio. In the mid and the long period bands, the maximum amplifications occur at the characteristic periods of the hills. As can be seen, increasing the shape ratio increases the characteristic period of the hill and its corresponding amplification factor. Figure 7 approximates the maximum amplification factor of the crest of 2D hills averaged over the Poisson ratio range of 0.1 to 0.4, as the following simple linear function of the shape ratio:

$$A_{\text{crest}} = 1 + 1.1\,(SR). \tag{3}$$

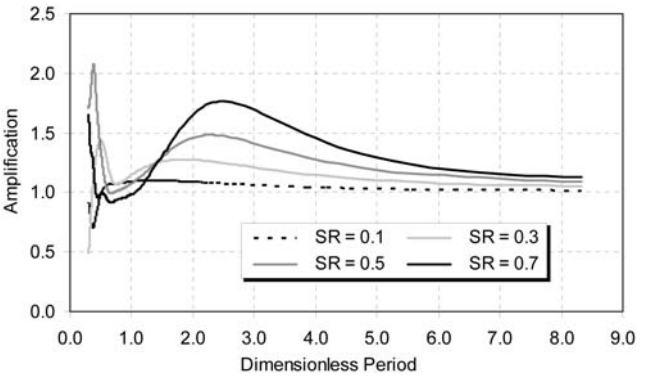

Figure 6. Incidence of a vertically propagating plane SV wave. Amplification curves of the crest of 2D trapezoidal hills with a Poisson ratio of 0.33 *versus* shape ratio.

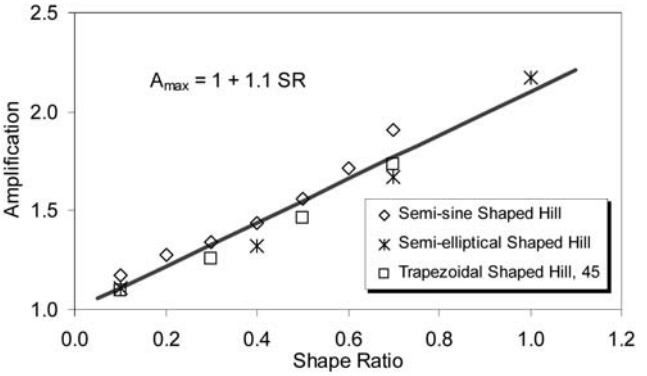

Figure 7. Incidence of a vertically propagating plane SV wave. The relation between maximum amplification factor at the crest of 2D semi-sine, semi-elliptical and trapezoidal shaped hills and shape ratio; averaged over the Poisson ratio range of 0.1 to 0.4.

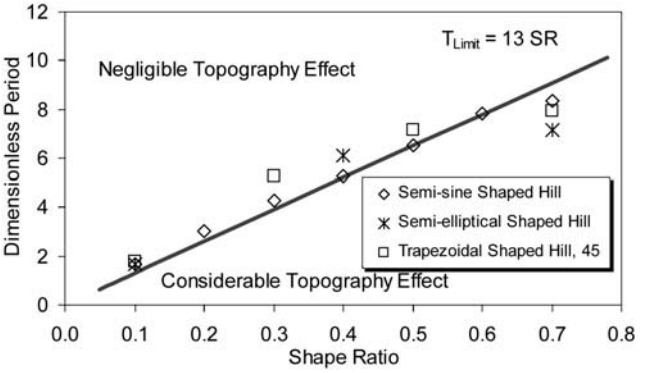

Figure 8. Incidence of a vertically propagating plane SV wave. The relation between limiting dimensionless period and shape ratio. In the areas above the line, the amplification effect of 2D hills could be practically ignored; that is, the amplification is equal or less than 1.1.

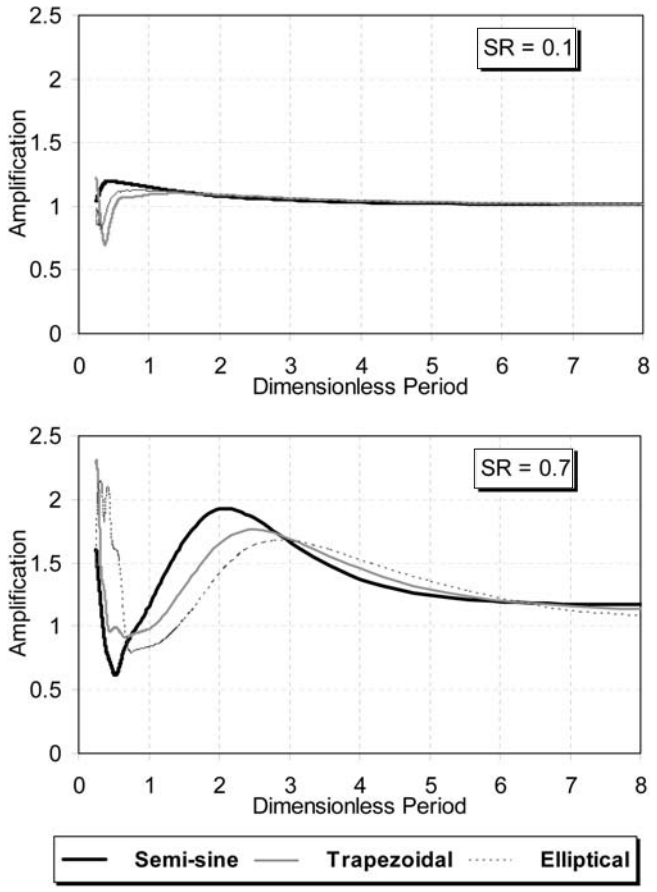

Figure 9. Incidence of a vertically propagating plane SV wave. Amplification curves at the crest of trapezoidal, semi-sine and semi-elliptical shaped hills, considering two limiting shape ratios of 0.1 and 0.7 and a Poisson ratio of 0.33.

Figure 8 estimates the limiting dimensionless period (wavelength) of vertically propagating incident SV waves producing an amplification factor of 1.1 at the crest of the 2D hills. These limiting periods are averaged over the Poisson ratio range of 0.1 to 0.4 and can be given as linear function of shape ratio of the hill:

$$T_{\text{limit}} = 13\,(SR). \tag{4}$$

If the incident waves possesses a predominant dimensionless period (wavelength) of greater than the limiting one (T_{limit}), the amplification potential at the crest would be less than 10 per cent and the topography effect could be practically ignored.

4.3 *Shape effect of the hill*

Figure 9 compares the amplification curves of the crest of trapezoidal, semi-sine and semi-elliptical shaped hills. The curves are obtained for two limiting shape ratios of 0.1 and 0.7 and a Poisson ratio of 0.33. Figure 10 compares the amplification curves corresponding to the defined five periodic sub-intervals. These curves are obtained along the trapezoidal, semi-sine and semi-elliptical shaped hills. Both figures show that the shape effect can play an important role in separating the amplification patterns of hills having similar shape ratios, depending on the wavelength of the incident wave. Hills that possess greater cross section areas (figure 2) have greater characteristic periods and corresponding amplification factors of less magnitude. In the case of incident waves with very long wavelengths, where the predominant periods are greater than the characteristic period of the hill, the shape effect could be simply ignored. In incident waves with short to long wavelengths, hills which have intermediate cross section areas demonstrate intermediate seismic behaviors, too. In other words, the ground response at any point along the hill would be governed by the whole topography instead of the local geometry around its vicinity. For example, in a trapezoidal hill with an intermediate cross section area and a shape ratio of 0.7, the amplification curves lay between those corresponding to the semi-sine and semi-elliptical shaped ones. On the other hand, in hills with shape ratio of 0.1, in which the semi-elliptical shaped hill has an intermediate cross section area, its amplification curves lay between those of the trapezoidal and semi-sine shaped ones. At last, in incident waves with very short lengths, where the predominant periods are much lower than the characteristic period of the hill, the amplification behavior of any point along the hill would be much more affected by the local geometry of its vicinity than the complete geometry of the whole hill.

Figures 11 and 12 demonstrate the variation of characteristic period and cross section area of the above-mentioned hills with shape ratio, respectively. Comparison of these figures confirms once again that among 2D hills with similar shape ratio, those with intermediate cross section areas have intermediate characteristic periods. In comparison between hills, as expected for each shape ratio, the semi-sine shaped hill with the least cross section area possesses also the least characteristic period. In hills with a shape ratio of approximately 0.4, the trapezoidal and semi-elliptical shaped hills, which have equal cross section areas, possess also equal characteristic periods. In hills with a shape ratio of less than 0.4, the trapezoidal hill, which has a larger cross section area compared to the semi-elliptical shaped one, possesses also a greater characteristic period. Finally, in hills with a shape ratio of greater than 0.4, the semi-elliptical shaped hill, which has a greater cross section area compared to the semi-elliptical shaped one, possesses also a greater characteristic period.

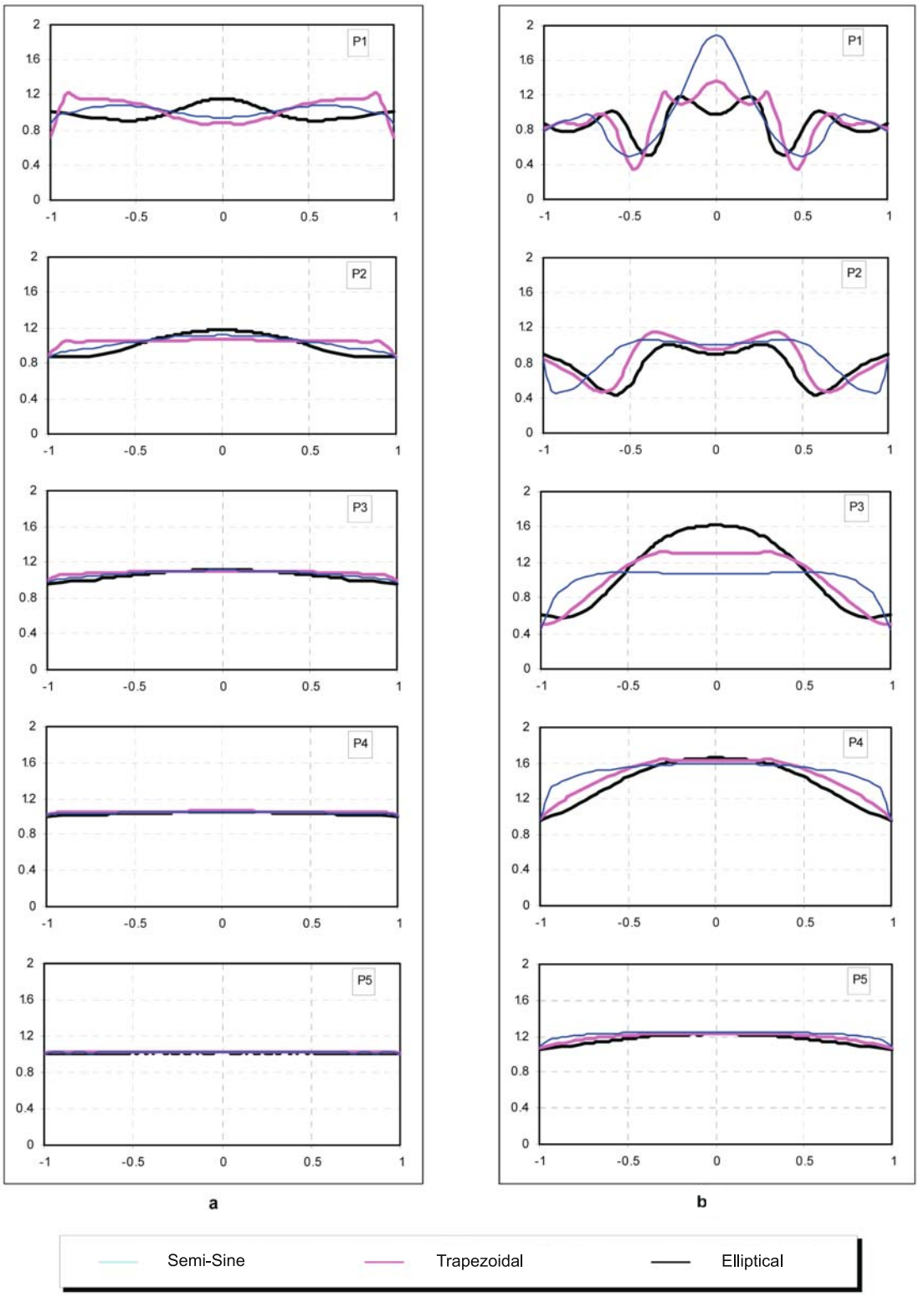

Figure 10. Incidence of a vertically propagating plane SV wave. Comparison of the shape effects on the amplification curves of the crest and rim of 2D semi-sine, semi-elliptical and trapezoidal shaped hills with a Poisson ratio of 0.33 and two limiting shape ratios of 0.1 and 0.7. The comparisons are made for five periodic sub-intervals.

4.4 *Poisson ratio effect*

Figure 13 demonstrates the effect of Poisson ratio variations on the amplification potential of the crest of 2D semi-sine shaped hills subjected to vertically propagating incident SV waves. As can be seen, the Poisson ratio has a secondary effect on the amplification potential of the hill, compared to

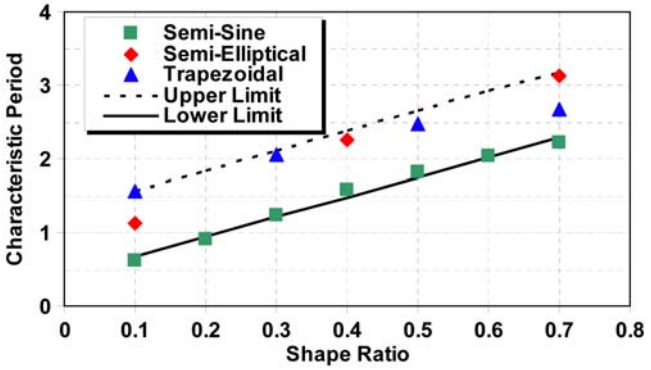

Figure 11. Characteristic periods of the semi-sine, semi-elliptical and trapezoidal shaped hills *versus* shape ratio (solid points). Two straight lines also indicate the upper and lower limits of characteristic periods for the hills. The characteristic periods are estimated for the incidence of a vertically propagating plane SV wave and for the hills with a Poisson ratio of 0.33.

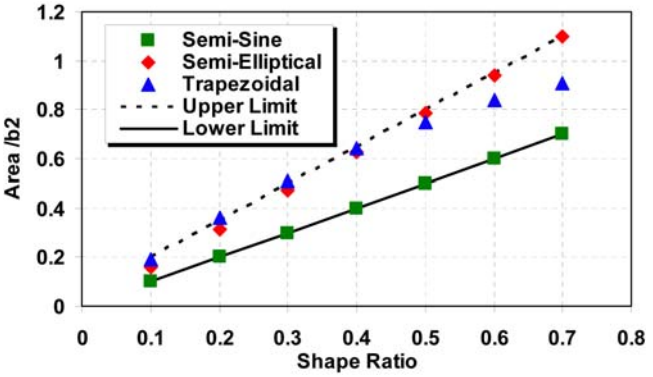

Figure 12. Cross section areas of the semi-sine, semi-elliptical and trapezoidal shaped hills *versus* shape ratio (solid points). Two straight lines also indicate the upper and lower limits of cross section areas for the hills.

the wavelength of the incident wave, shape ratio and shape effect of the hill. In the case of hills with small shape ratios (< 0.2), the Poisson ratio effect could actually be ignored, regardless of the incident wavelength. In the case of hills with greater shape ratios, unless the incident wave possesses a medium or smaller wavelength, the Poisson ratio effect could also be ignored. As expected for incident waves with predominant periods of higher than the characteristic period, the amplification factor decreases as the Poisson ratio increases.

5. Seismic site coefficients

The results presented so far in this paper indicate that considering all homogenous rocky sites as similar amplification-free reference sites is neither reasonable nor conservative. However, this site classification is being done in the current practice of seismic microzonation studies for every point of ground surface, irrespective of being located on the toe or top of the hill (points C and D in figure 1) or on the flat half-plane (point B in figure 1). The obtained results encourage one to go a new step forward in seismic microzonation of areas with topographical structures by distinguishing conservatively, the seismic behavior of homogenous hills and that of the free field half-plane.

Tables 2 and 3 approximate the average horizontal spectra amplification factors (AHSA) of the crest and toe of a 2D homogenous elliptical shaped hill subjected to vertically propagating incident SV waves, respectively. The amplification factors are calculated as functions of the shape-ratio and the predominant dimensionless period. The Poisson ratio is considered to be 0.33 which is a typical value for hills. Using such tables enables one not only to prepare distribution maps of period dependent site amplification factors throughout a study area, but also to estimate conservative values of the well-known short period (F_a) and long period (F_v) site coefficients required for evaluating proper design spectra for structures located on rocky hills (figure 14). The extensive experimental studies conducted by Borcherdt *et al* (1991); Borcherdt (1994) showed that the short period site coefficient could be approximated as the spectral amplification averaged over the period interval 0.1 to 0.5 s, whereas the long period site coefficient could be approximated as the spectral amplification averaged over the period interval 0.4 to 2.0 s. The spectral amplification was simply defined as ratio of the Fourier amplitude of the ground motion (point A in figure 1) to the Fourier amplitude of the rocky reference site motion (point B in figure 1).

Following Borcherdt's empirical idea, tables 2 and 3 could be simply used in order to evaluate conservatively the crest and toe (points D and C in figure 1) spectral amplification with respect to rocky reference site (point B in figure 1), averaged over the above-mentioned short and long period intervals. Considering a 2D elliptical shaped hill with a shear wave velocity of 1000 m/s and a width interval of 100 to 1000 meters, figure 15 demonstrates the dimensionless period bands (P1 to P5) encountered in averaging the spectral amplification over the period intervals 0.1 to 0.5 as well as 0.4 to 2.0 s.

Tables 4 and 5 demonstrate the short and long period site coefficients of crest and toe of the above-mentioned 2D elliptical shaped hill as a function of its shape ratio and width. The values of these tables have been calculated using a weighted averaging procedure. As an example, considering a 200 m width hill, the long period interval (0.4 to 2.0 s) encounters the dimensionless periodic bands

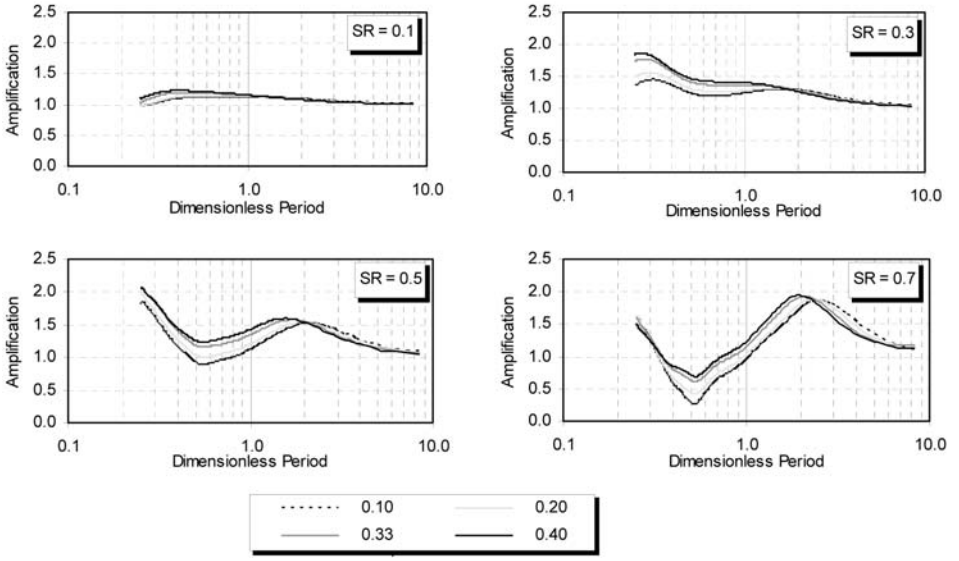

Figure 13. Incidence of a vertically propagating plane SV wave. Effect of Poisson ratio on the amplification curves of the crest of the semi-sine shaped hills *versus* different shape ratios. The vertical axis depicts the ratio of the cross section area of the hill to its square half width, while the horizontal axis shows the shape ratio.

Table 2. *Horizontal amplification factors of crest.*

	Dimensionless periodic range				
SR	P1	P2	P3	P4	P5
0.1	1.0	1.1	1.1	1.1	1.0
0.4	1.5	1.3	1.3	1.3	1.1
0.7	1.9	1.1	1.1	1.6	1.2
1.0	1.8	1.0	1.0	1.9	1.7

Table 3. *Horizontal amplification factors of toe.*

	Dimensionless periodic range				
SR	P1	P2	P3	P4	P5
0.1	1.0	1.0	1.0	1.0	1.0
0.4	1.0	1.0	1.0	1.1	1.1
0.7	1.0	1.0	1.0	1.1	1.1
1.0	1.1	1.0	1.0	1.0	1.2

P4 and P5, which results in average horizontal amplification factors 1.7 and 1.1 respectively for crest and toe of an elliptical hill, assuming a shape ratio of 1.0.

It is worth noting that practically, there is no amplification in the 2D semi-elliptical shaped hills with shape ratio less than 0.1. Moreover, the amplification is negligible in the toe of the elliptical hills, both in short and long periods; that is, the amplification value is less than 1.1, and there is a much lower concern with these areas. However, in the crest and adjacent regions of crest of mentioned hills the amplification is significant and varies with the period. The site coefficients of crest varying

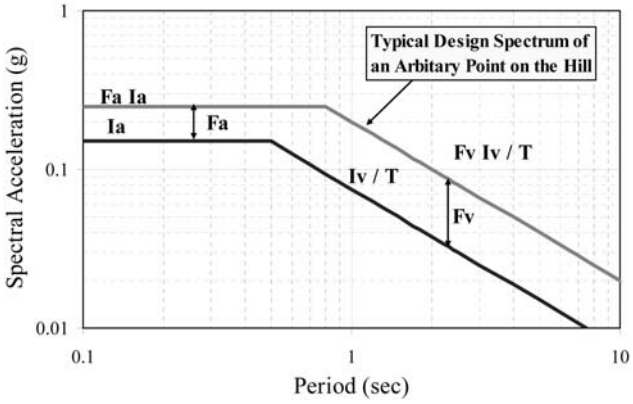

Figure 14. Schematic design spectrum of 2D rocky hills in terms of short period (I_a) and long period (I_v) seismic hazard levels as well as short period (F_a) and long period (F_v) spectral amplification factors.

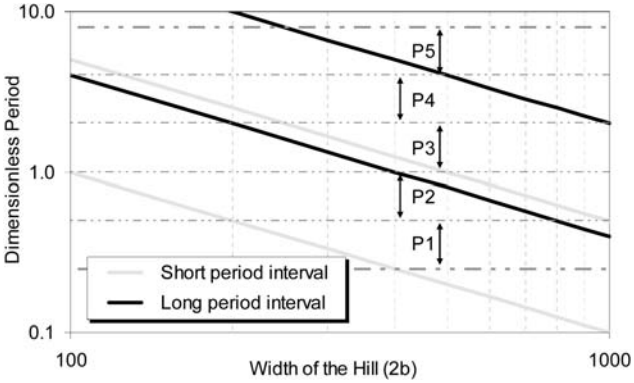

Figure 15. Dimensionless period bands (P1 to P5) encountered in averaging the spectral amplification over the short period (0.1 to 0.5 s) and long period (0.4 to 2.0 s) intervals, assuming shear wave velocity of 1000 m/s.

Table 4. *Short and long period coefficients of 2D elliptical hill's crest with shear wave velocity of 1000 m/s.*

	Hill width (2b)					
	100–300		400–700		800–1000	
SR	F_a	F_v	F_a	F_v	F_a	F_v
0.1	1.1	1	1.1	1.1	1	1.1
0.4	1.3	1.2	1.4	1.3	1.5	1.3
0.7	1.3	1.3	1.5	1.4	1.7	1.2
1.0	1.3	1.7	1.4	1.5	1.6	1.1

Table 5. *Short and long period coefficients of 2D elliptical hill's toe with shear wave velocity of 1000 m/s.*

	Hill width (2b)					
	100–300		400–700		800–1000	
SR	F_a	F_v	F_a	F_v	F_a	F_v
0.1	1	1	1	1	1	1
0.4	1	1.1	1	1.1	1	1
0.7	1	1.1	1	1.1	1	1
1.0	1	1.1	1.1	1	1.1	1

between 1.0 and 1.7 are comparable to the 1D site coefficients usually recommended by the worldwide standard seismic codes such as UBC97 and IBC2006 for site classes C and D. Besides, in some locations these coefficients exceed the maximum value of 1.4 proposed by the AFPS (1990) code for seismic design of structures in topographic areas. Also, the site coefficients proposed by tables 4 and 5 are period dependent and therefore more representative of the amplification pattern of 2D hills, whereas the constant topography factors proposed by AFPS (1990) and Eurocode 8 (1998) do not take this important controlling factor into account.

6. Conclusion

This paper presents clear perspectives of amplification patterns of 2D homogenous trapezoidal, semi-sine and semi-elliptical shaped hills subjected to vertically propagating SV incident waves. The results are obtained by an extensive numerical parametric analysis using the time domain boundary element method. Preliminary relations and tables are proposed which could be used as starting points in the estimation of important engineering indexes in seismic microzonation studies of areas with topographic structures. It is shown that:

- The amplification potential of the hill is strongly influenced by the length of the incident wave, by the shape ratio, by the shape of the hill and in a less order of importance, by the Poisson ratio of the media.
- Every hill has a characteristic period that controls its seismic response. If the incident wave has a predominant period equal to the characteristic one, all points along the hill show in-phase motions and its amplification potential reaches the maximum at the crest.
- In the case of incident waves with wavelengths longer than the width of the hill, where the predominant periods are usually equal to or greater than its characteristic period, the amplification curve reaches the maximum at the crest and decreases towards the base of the hill. In incident waves with smaller wavelengths, some deamplification zones would exist along the hill and the maximum amplification potential could even occur along the flank.
- Although the amplification potential of the hill increases with the shape ratio, the increasing rate depends on the wavelength and varies across the hill. The maximum amplification factor along the hill occurs mostly at the crest and has an increasing rate of 1.1 times the increasing rate of the shape ratio.
- In case of incident waves with a wavelength of between 0.5 and 4 times the widths of the hill, the ground response at any point along the hill would be governed by the whole topography instead of the local geometry around its vicinity. Among hills with similar shape ratios, those with intermediate cross section areas show intermediate seismic behavior, too.
- The topography effect can be ignored, only if the hill has a shape ratio of less than 0.1 or is subjected to incident waves with wavelengths of greater than T_{limit} times its width. The coefficient T_{limit} can be estimated as 13 times the shape ratio.
- Estimated seismic site coefficients for the crest of 2D rocky hills vary between 1.1 and 1.7. The coefficients encourage one to classify a site, according to site standard categorization procedures, as soil profile types S_C and S_D instead of S_B, depending on the shape ratio.

Acknowledgements

The authors thank Prof. Mohammad Kazem Jafari and Prof. Mohammad Hassan Baziar for their valuable comments and discussions which played a key role in finalising this paper.

References

Aki K and Larner K 1970 Surface motion of a layered medium having an irregular interface due to incident plane SH waves; *J. Geophys. Res.* **75** 933–954.

Ashford S A, Sitar N, Lysmer J and Deng N 1997 Topographic Effects on the Seismic Response of Steep Slopes; *Bull. Seismol. Soc. Am.* **87** 701–709.

Association Française du Genie Parasismique (AFPS) 1990 *Recommandations de la AFPS.* Paris: AFPS, 183 pp.

Athanasopoulos G A, Pelekis PC and Leonidou E A 1999 Effects of Surface Topography on Seismic Ground Response in the Egion (Greece) 15-6-1995 Earthquake; *Soil Dynamics and Earthquake Engineering* **18** 135–149.

Bard P Y 1982 Diffracted waves and displacement field over two-dimensional elevated topographies; *Geophys. J. R. Astr. Soc.* **71** 731–760.

Beskos D E 1987 Boundary element methods in dynamic analysis; *Appl. Mech. Rev.* **40** 1–23.

Beskos D E 1997 Boundary element methods in dynamic analysis: Part II (1986–1996); *Appl. Mech. Rev.* **50(3)** 149–197.

Boore D M 1972 A note on the effect of simple topography on seismic SH waves; *Bull. Seismol. Soc. Am.* **62** 275–284.

Boore D M 1973 The effect of simple topography on seismic waves: implications for the accelerations recorded at Pacoima Dam, San Fernando Valley, California; *Bull. Seismol. Soc. Am.* **63** 1603–1609.

Borcherdt R D, Wentworth C M, Janssen A, Fumal T and Gibbs J 1991 Methodology for Predictive GIS Mapping of Special Study Zones for Strong Ground Shaking in the San Francisco Bay Region, California; *Proc. Fourth Int. Conference Seismic Zonational* (Stanford: California) 545–552.

Borcherdt R D 1994 Estimates of site-dependent response spectra for design (Methodology and Justification); *Earthquake Spectra* **10** 617–653.

Bouchon M 1973 Effect of Topography on Surface Motion; *Bull. Seismol. Soc. Am.* **63** 615–632.

Bouchon M 1985 A simple complete numerical solution to the problem of diffraction of SH waves by an irregular surface; *J. Acoust. Soc. Am.* **77** 1–5.

Bouckovalas G D and Kouretzis G 2001 Review of Soil and Topography Effects in the September 7, 1999 Athens (Greece) Earthquake; *Proc. Fourth Int. Conference on Recent Advances in Geotechnical Earthquake Engg. and Soil Dyn. and Symposium in Honor of Professor W D Liam Finn* (San Diego: California).

Bouckovalas G D and Papadimitriou A G 2005 Numerical evaluation of slope topography effects on seismic ground motion; *Soil Dynamics and Earthquake Engineering* **525** 547–558.

Celebi M 1987 Topographical and geological amplifications determined from strong-motion and aftershock records of the 3 March 1985 Chile earthquake; *Bull. Seismol. Soc. Am.* **77** 1147–1167.

Celebi M 1991 Topographic and geological amplification: Case studies and engineering implications; *Struct. Safety* **10** 199–217.

Eurocode 8 (EC8) 1998 *Design provisions for earthquake resistance of structures.*

Gaffet S and Bouchon M 1989 Effect of two-dimensional topographies using the discrete wavenumber-boundary integral equation method in P-SV cases; *J. Acoust. Soc. Am.* **83** 2277–2283.

Geli L, Bard P V and Julien B 1988 The effect of topography on earthquake ground motion: A review and new results; *Bull. Seismol. Soc. Am.* **78** 42–63.

International Council of Building Officials (ICBO) 2006 *International Building Code.*

International Council of Building Officials (ICBO) 1997 *Uniform Building Code.*

Kamalian M 2001 *Time Domain Two-Dimensional Hybrid FEM/BEM Dynamic Analysis of Non-Linear Saturated Porous Media*; Ph.D. thesis, Tehran University, Tehran, Iran.

Kamalian M, Gatmiri B and Sohrabi-Bidar A 2003a On Time-Domain Two-Dimensional Site Response Analysis of Topographic Structures by BEM; *J. Seismol. Earthquake Engg.* **5** 35–45.

Kamalian M, Jafari M K, Dehghan K, Sohrabi-Bidar A and Razmkhah A 2003b Two-Dimensional Hybrid Response Analysis of Trapezoidal Shaped Hills in Time Domain, *Advances in Boundary Element Techniques IV* (eds) Gallego R and Aliabadi M H, 231–236.

Kamalian M, Jafari M K, Sohrabi-Bidar A, Razmkhah A and Gatmiri B 2006 Time-Domain Two-Dimensional Site Response Analysis of Non-Homogeneous Topographic Structures by A Hybrid FE/BE Method; *Soil Dynamics and Earthquake Engineering* **26** 753–765.

Kamalian M, Gatmiri B, Sohrabi-Bidar A and Khalaj A 2007 Amplification Pattern of 2D Semi-Sine Shaped Valleys Subjected to Vertically Propagating Incident Waves; *Commun. Numer. Meth. Engg.* **23** 871–887.

Moczo P, Bystricky E, Kristek J, Carcione J M and Bouchon M 1997 Hybrid modeling of P-SV seismic motion at inhomogeneous viscoelastic topographic structures; *Bull. Seismol. Soc. Am.* **87** 1305–1323.

Pedersen H A, Sánchez-Sesma F J and Campillo M 1994 Three-dimensional scattering by two-dimensional topographies; *Bull. Seismol. Soc. Am.* **84** 1169–1183.

Sánchez-Sesma F J 1983 Diffraction of elastic waves by three-dimensional surface irregularities; *Bull. Seismol. Soc. Am.* **73** 1621–1636.

Sánchez-Sesma F J 1987 Site effects on strong ground motion; *Soil Dynamics and Earthquake Engineering* **6** 124–132.

Sánchez-Sesma F J and Campillo M 1991 Diffraction of P, SV and Rayleigh waves by topographic features: A boundary integral formulation; *Bull. Seismol. Soc. Am.* **81** 2234–2253.

Sánchez-Sesma F J and Campillo M 1993 Topographic effects for incident P, SV and Rayleigh waves; *Tectonophys.* **218** 113–125.

Sánchez-Sesma F J, Palencia V J and Luzon F 2002 Estimation of local site effects during earthquakes: An overview; *ISET Journal of Earthquake Technology* **39** 167–193.

Spudich P, Hellweg M and Lee W H K 1996 Directional topographic site response at Tarzana observed in aftershocks of the 1994 Northridge, California, Earthquake: Implications for mainshock motions; *Bull. Seismol. Soc. Am.* **86** S139–S208.

Takenaka H, Kennett B L N and Fujiwara H 1996 Effect of 2-D topography on the 3-D seismic wavefield using a 2.5-dimensional discrete wavenumber – boundary integral equation method; *Geophys. J. Int.* **124** 741–755.

The Technical Committee for Earthquake Geotechnical Engineering (TC4) 1993 *Manual for Zonation on Seismic Geotechnical Hazard*; The Japanese Society of Soil Mechanics and Foundation Engineering.

Trifunac M D and Hudson D E 1971 Analysis of the Pacoima Dam accelerograms – San Fernando earthquake of 1971; *Bull. Seismol. Soc. Am.* **61** 1393–1411.

Zhang B, Papageorgiou A S and Tassoulas J L 1998 A hybrid numerical technique, combining the finite-element and boundary-element methods, for modeling the 3D response of 2D scatterers; *Bull. Seismol. Soc. Am.* **88** 1036–1050.

Zhang C and Zhao C 1988 Effects of canyon topography and geological conditions on strong ground motion; *Earthquake Engg. Structural Dyn.* **16** 81–97.

Zhao C and Valliappan S 1993 Incident P and SV wave scattering effects under different canyon topographic and geological conditions; *Int. J. Numer. Anal. Meth. Geomech.* **17** 73–94.

MS received 22 September 2007; revised 17 January 2008; accepted 22 April 2008